

THE EFFECT OF PYLON TRAILING EDGE BLOWING ON THE PERFORMANCE AND NOISE PRODUCTION OF A PROPELLER

L.L.M. Veldhuis* , T. Sinnige*
*Delft University of Technology

Keywords: *propeller flow, noise, pylon interaction, trailing edge blowing, flow control*

Abstract

This paper discusses a study of the effects of pylon trailing edge blowing on pusher propeller performance and noise emissions. Experimental investigations were performed in a low speed open jet wind tunnel, using a powered propeller model and a generic pylon model. A novel pylon blowing system was integrated in the aft part of the pylon to provide a uniform outflow. The numerical analysis was executed using a combination of a propeller model that is based on an extended Blade Element Model (BEM) and a set of analytic methods from the literature, to assess the effects of pylon installation on the propeller performance and noise emissions. Measurements of the velocity distributions in the blown pylon wake showed that application of the blowing system reduced the integrated velocity deficit by up to 60% compared to the unblown configuration. Evaluations of the propeller forces and moments showed that the effects of installation on the time-averaged propeller performance are small, with differences of at most 2% for advance ratios below $J=1.4$. Furthermore, excellent agreement was obtained between the computed and measured performance for the isolated propeller. With respect to the propeller noise emissions it was observed that installation of the pylon upstream of the propeller strongly increases the noise levels. Depending on the propeller operating point, noise penalties of up to 15dB were measured. The application of pylon blowing clearly reduced the propeller noise emissions

over the entire advance ratio range, with reductions of up to 7dB compared to the unblown case. The largest noise reductions were found at the highest blowing rate, indicating that the most effective blowing rate might not have been reached yet.

1 Introduction

The environmental impact of aircraft operations and increasing fuel prices have led to the demand for more fuel-efficient aircraft. One of the technologies with the potential to offer a significant reduction in fuel burn is the open rotor engine, which allows the bypass ratio to be increased to values unattainable by turbofans. This results in a step change in propulsive efficiency, with estimations for the corresponding reduction in fuel burn at around 25 – 30% [11, 17, 26]. The major disadvantage of the open rotor engine is its associated high level of noise emissions. In case of a contra rotating open rotor (CROR) configuration, tonal noise is generated by each rotor individually as well as by the aerodynamic interactions between the two rotors. In addition to isolated noise sources, installation of the open rotor on the aircraft introduces another noise generating mechanism. For interior noise and ground clearance reasons, a pylon-mounted placement at the aft end of the fuselage, with a pusher configuration is considered in most of the studies presented in the literature. In this case the wake shed from the upstream pylon impinges on the front rotor, resulting in unsteady blade loading and associated noise emissions [2, 3, 10, 12, 17, 19, 23].

The pylon - open rotor interaction mainly affects the noise levels associated with the front rotor tones, while the rear rotor tones show only a small effect and the interaction tones remain unaffected [18, 19, 23, 25]. Furthermore, apart from the impact on the propeller noise emissions, the fluctuating blade loads may also affect the propeller performance.

2 Pylon Trailing Edge Blowing

The pylon installation effects originate from the impingement of the pylon wake on the propeller. The resulting non-uniform propeller inflow leads to unsteady blade loading with associated performance and noise emission penalties. Based on the interaction mechanism it can be expected that the installation effects can be reduced or even completely removed by eliminating the pylon wake. Ricouard et al. [19] show that especially the active technique of pylon blowing can be very effective in reducing the pylon - propeller interaction effects.

The concept of pylon wake elimination through pylon blowing is illustrated in Fig.1, which presents an idealized example in which the pylon wake is filled up completely.

The potential of pylon trailing edge blowing to reduce the adverse installation effects experienced on rear-fuselage mounted open rotor engines forms the main topic of this paper. Both experimental and numerical investigations were performed. It should be noted that the available experimental equipment limited the current study to single-rotating propeller applications, in con-

trast to the contra-rotating technology typically projected for future applications of open rotor engines on next-generation passenger aircraft.

3 Experimental Setup

The experiments were performed in a low speed open jet wind tunnel, using a powered propeller model and a typical pylon model. A novel "Uniform Blowing Rod" (UBR) was integrated in the aft part of the pylon. A number of measurement techniques were applied to measure the pylon wake profiles, propeller performance, and propeller noise emissions.

3.1 Wind Tunnel Facility

All experiments were performed in Delft University of Technology's Open Jet Facility (OJF) [6]. This closed circuit wind tunnel with open test section has an octagonal outlet with width and height equal to 2.85 m and provides a maximum wind velocity of 32 m/s. To remove spatial velocity deviations and to reduce the flow's turbulence level, the settling chamber is equipped with a honeycomb flow rectifier and five screens. This results in velocity deviations smaller than 0.5% in the vertical plane at 2 m from the outlet, with a longitudinal turbulence intensity level around 0.24%. To reduce noise levels, the inside of the entire tunnel is covered with perforated plates installed on mineral wood and sound absorbing foam. The fan however does not feature any special noise reduction measures.

3.2 Wind Tunnel Models

The wind tunnel tests involved the use of two scale models: a powered propeller and a pylon. To simulate a pusher configuration the tractor propeller model was placed behind the pylon.

3.2.1 Propeller Model

The powered single-rotating propeller scale model was made by Fokker Aircraft Company during the development of the conceptual Fokker F29. The model has a diameter of $D_{prop} = 0.3043$ m, a hub diameter of $D_{hub} = 0.084$ m, and is equipped with up to eight blades. In the

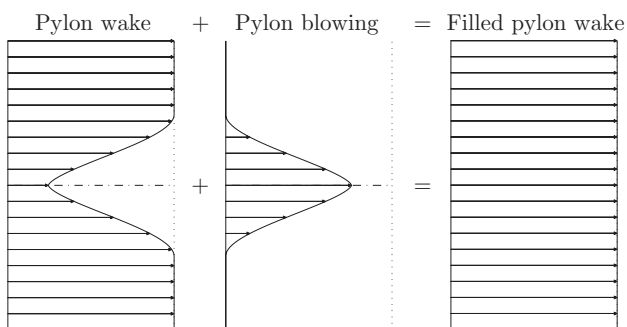


Fig. 1 Schematic illustrating the concept of pylon wake elimination through pylon blowing.

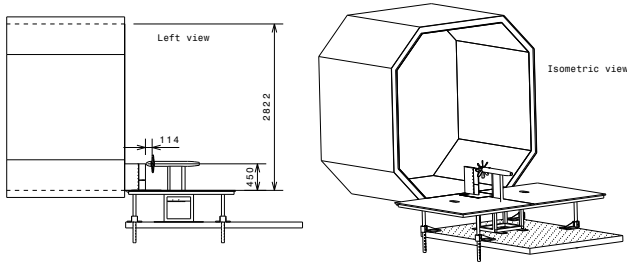


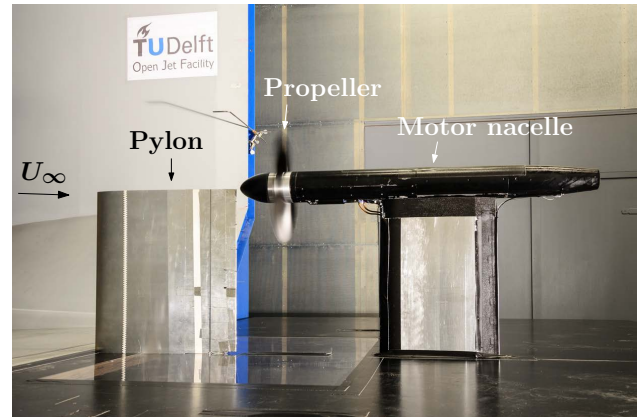
Fig. 2 Overview of the installed propeller setup (dimensions in millimeters).

current study the eight-bladed configuration was selected. The blade angle at 75% of the blade span can be adjusted as desired, and was set to $\beta_{0.75R} = 41^\circ$. The propeller is driven by a Tech Development (TDI) 1999A pneumatic motor. A four-component Rotating Shaft Balance (RSB), capable of separately measuring thrust, torque and in-plane components, is integrated in the propeller model. The entire propeller test rig is utilized and maintained by Delft University of Technology and it is obtained from the German-Dutch Wind Tunnels (DNW) on a lease basis.

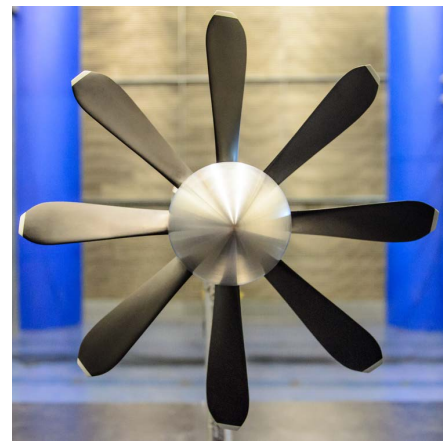
The propeller model was positioned at 30% of the pylon chord behind the pylon during the measurements performed in the installed and blown configurations. Note that this spacing is at the high end of the spectrum of pylon - propeller spacings considered during comparable pylon - propeller interaction studies available in the literature [2, 3, 4, 13, 23, 25, 28]. However, taking into account the geometry of the powered propeller model it was not possible to position the propeller any closer to the pylon. A technical drawing of the complete setup of the propeller in the installed configuration is presented in Fig. 2. Photographs of the propeller test setup in the OJF wind tunnel are shown in Fig. 3.

3.2.2 Pylon Model

The pylon was designed based on typical pylon characteristics used in comparable pylon - propeller interaction studies [2, 3, 4, 13, 23, 25, 28] and taking into account the minimum dimensions required for a successful integration of the blowing system in the trailing edge region of the pylon. As a result, the pylon had a straight, unta-



Side view



Eight-bladed propeller in close-up

Fig. 3 Propeller-Pylon setup in the Delft University OJF windtunnel.

pered planform with the cross-section formed by a NACA 0012 profile modified to have a trailing edge thickness of 1.1% of the chord. The pylon chord length was equal to 1.33 times the propeller diameter, while the span of the pylon was selected based on the available space in the test setup, resulting in a span of $b_{pyl} = 0.450$ m. Transition was fixed at 25% of the chord at both sides of the pylon.

An overview of the pylon characteristics is given in Table 1; a technical drawing of the pylon model is depicted in Fig. 4.

3.3 Uniform Blowing Rod

The core of the pylon blowing system is formed by a Uniform Blowing Rod (UBR). Developed

Table 1 Pylon model characteristics.

Parameter	Symbol	Value
Chord	c_{pyl}	$1.33/D_{prop}$
Span	b_{pyl}	$1.48/D_{prop}$
TE thickness	t_{TE}	$0.011/c$
Sweep angle	Λ_{pyl}	0°
Taper ratio	λ_{pyl}	1.0
Airfoil	-	NACA 0012 (mod)

in conjunction with FlowMotion¹, the UBR is designed to provide a uniform outflow from its outlet. The UBR basically consists of two components: an interior air channel with a variable cross-sectional shape along the span, and an outlet channel with a constant cross-section and vanes placed at constant spacing to align the flow which exits the UBR.

The UBR design is characterized by the geometry of the initial cross-section (at the inlet plane, i.e. the UBR's root), after which the shape of the cross-sections of the interior air channel in spanwise direction towards the tip are computed such that in theory a uniform outflow profile is obtained. This is done by taking into account the boundary layer development along the UBR's interior air channel in determining the optimal local cross-sections. A simple rectangle was chosen as cross-section at the root of the UBR. Vanes are placed in the outlet segment to align the flow before it exits the UBR. The final shape of the vanes was determined based on analyses of the UBR's outflow profiles performed with ANSYS Fluent using steady-state RANS simulations of the flow inside the UBR. A technical drawing of the final UBR design, as integrated in the aft part of the pylon, is presented in Fig. 5.

3.4 Measurement Techniques

3.4.1 Pressure measurements

The wake profiles behind the unblown and blown pylons were measured by traversing a total and a static pressure tube over a range of lateral positions behind the pylon. During all measurements

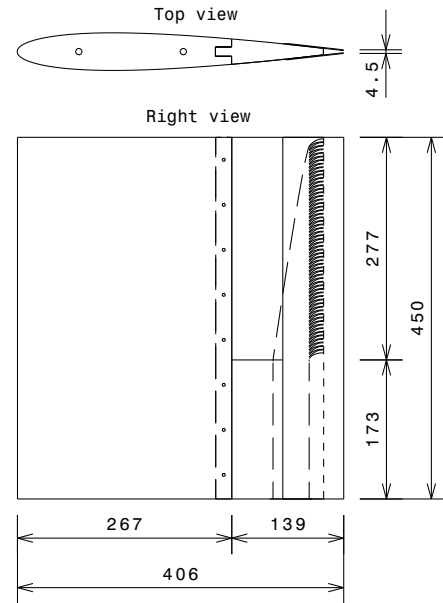


Fig. 4 Geometry of the pylon model (dimensions in millimeters).

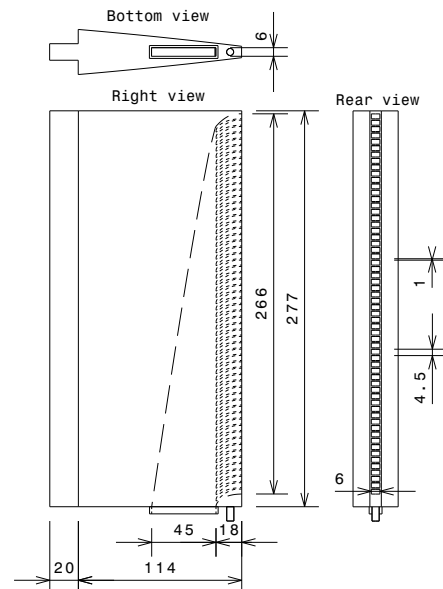


Fig. 5 Uniform Blowing Rod (UBR) geometry (dimensions in millimeters).

¹FlowMotion - Consultancy for Heat Transfer and Fluid Dynamics: www.flowmotion.nl

the pylon was set to zero degrees angle of attack. The tubes were installed on a computer controlled traversing system which could translate in all three directions.

3.4.2 Noise measurements

Two LinearX M51 high performance low voltage electret condenser microphones were used to measure the acoustic pressures induced during the experiments. Both microphones were positioned outside the open jet stream, at a sideline distance of 2.25 m from the centerline of the propeller. The frequency response of the microphones is practically flat in the 50-2000 Hz range; for the response at lower and higher frequencies calibrated correction factors provided by LinearX were used to correct the microphone data. Furthermore, a correction was applied to account for refraction effects due to the presence of the shear layer following the method outlined in Ref. [16]. The microphone measurements were performed at the same sampling frequency as used for the RSB measurements: 50 kHz. To convert the raw microphone signals into sound pressure levels the microphones were calibrated every measurement day using a pistonphone.

3.4.3 Particle image velocimetry

A stereoscopic PIV system was used to measure the velocity fields around the propeller blades at several radial stations. The laser light was provided by a Qantel EverGreen CFR200 Nd:Yag laser with a pulse energy of 200 mJ/pulse. Tracer particles were introduced downstream of the wind tunnel test section with a SAFEX Twin Fog generator using a SAFEX inside nebelfluide mixture of diethylene glycol and water. Two LaVision Imager Pro LX 16 Mpix (4,872 x 3,248 pixels) cameras were used with Nikon 105mm f/2.8 AF Micro lenses (set to f/5.6-8) to record the image pairs. Data sets consisting of 200 image pairs were recorded phase-locked at a measurement frequency of about 0.5 Hz.

A photograph depicting an overview of the PIV setup is presented in Fig. 6.

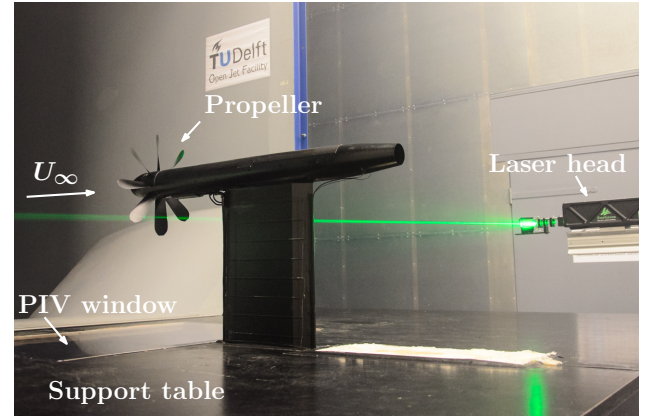


Fig. 6 Overview of PIV setup.

4 Numerical Setup

A numerical scheme was developed to compute the effects of pylon installation on the performance and noise emissions of pusher propellers, following the schematic flowchart depicted in Fig. 7.

4.1 Pylon Wake Profiles

To compute the effects of installation of the pylon on the propeller performance and noise emissions the pylon wake profiles need to be determined first. For this purpose the Schlichting wake model was used, which is characterized by the following two governing equations (Ref. [20]):

$$\frac{\Delta u}{U_\infty}(X_w, Y_w) = \frac{\sqrt{10}}{18\beta} \sqrt{\frac{c_d c}{X_w}} \left[1 - \left| \frac{Y_w}{b} \right|^{\frac{3}{2}} \right]^2 \quad (1)$$

$$b_w(X_w) = \beta \sqrt{10 c_d c X_w} \quad (2)$$

with b_w the wake semi-width, c the chord length, c_d the pylon 2D drag coefficient, Δu the local velocity deficit in the pylon wake, U_∞ the freestream velocity, X_w and Y_w longitudinal and lateral coordinates measured from the center of the pylon's trailing edge, and β an empirical constant equal to $\beta = 0.18$ [20]. The pylon drag coefficient was computed using XFOIL [7].

Note that the blown pylon wake profiles cannot be computed using the developed numerical tool. Instead, for the computations related to the

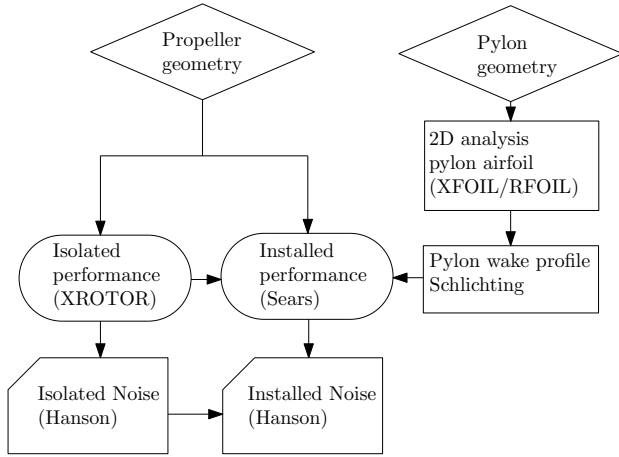


Fig. 7 Flowchart of the numerical scheme developed to analyze pusher propeller performance and noise emissions.

blown configuration wake profiles were used as obtained from the experimental evaluations.

4.2 Propeller Performance

The numerical assessment of the propeller performance is built around the propeller analysis and design program XROTOR [8]. The installation effects are accounted for by correcting the isolated blade response for the change in the dynamic pressure and the angle of attack in the pylon wake.

4.2.1 Isolated Configuration

The isolated (steady-state) propeller performance was computed using the propeller lifting line program XROTOR. The propeller blade section characteristics which are required as inputs to XROTOR were determined using RFOIL [27]. To correct for the effects of rotation on the blade section characteristics the empirical model developed by Snel et al. was used (Ref. [24]):

$$c_l^{\text{rot}} = c_l + \tanh \left\{ A \left(\frac{c}{r} \right)^B \right\} (c_l - c_{l_{\text{lin}}}) \quad (3)$$

with A and B tuning parameters, set to their default values of $A = 3$ and $B = 2$, respectively [24]. The drag coefficient was not corrected for rotational effects.

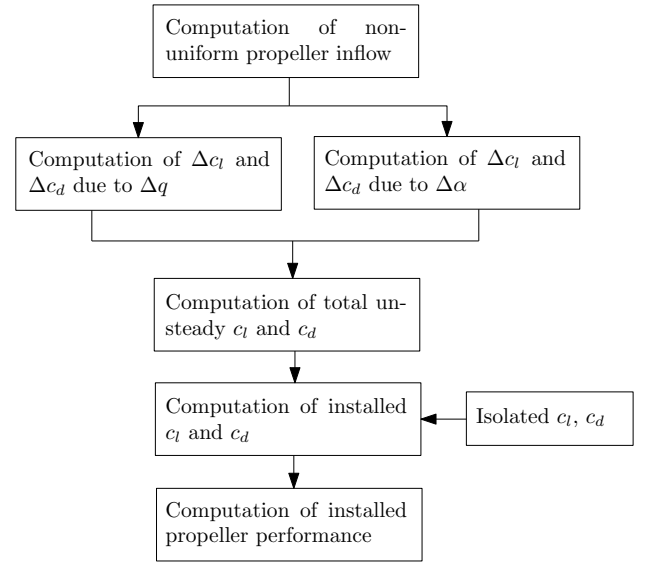


Fig. 8 Flowchart of the installed propeller performance computation routine.

4.2.2 Installed Configuration

Following the isolated performance computations the installation effects for a single-rotating pusher propeller are considered. In the installed configuration the inflow at the propeller disk is characterized by a non-uniform velocity field due to the velocity deficit in the pylon wake. The assumption is made that the final installed blade loading can be computed by following the principle of superposition, hence the effects of the changes in the dynamic pressure and the angle of attack are considered separately. A flowchart of the installed propeller performance computation routine is presented in Fig. 8.

The change in blade loads due to the varying dynamic pressure is evaluated at the local angles of attack computed for the isolated case. The assumption is made that the isolated lift and drag coefficients per radial station are constant over the full rotation, hence Reynolds number effects are neglected. Furthermore, it is assumed that the induced velocities corresponding to the steady-state solution apply at each polar angle ϕ without modification. The changes in the lift and drag coefficients due to the variation in dynamic pressure at constant angle of attack $\Delta c_{l_{\text{inst}}}^{\Delta q}$ and $\Delta c_{d_{\text{inst}}}^{\Delta q}$ are computed using:

$$\Delta c_{l_{inst}}^{\Delta q}(\eta, \phi) = c_l^{SS}(\eta) \left\{ \frac{W_{inst}^2(\eta, \phi)}{W_{iso}^2(\eta)} - 1 \right\} \quad (4)$$

$$\Delta c_{d_{inst}}^{\Delta q}(\eta, \phi) = c_d^{SS}(\eta) \left\{ \frac{W_{inst}^2(\eta, \phi)}{W_{iso}^2(\eta)} - 1 \right\} \quad (5)$$

with c_l^{SS} and c_d^{SS} the steady-state (isolated) lift and drag coefficients, W_{iso} the undisturbed effective velocity, W_{inst} the local effective velocity in installed conditions, η the non-dimensional radial coordinate, and ϕ the polar angle.

The change in blade loads due to the variation of the angle of attack in the pylon wake region is computed using Sears' method, which is described in Refs. [21, 22]. Only the lift coefficient is considered; the effects on the drag coefficient are neglected. The computation of the unsteady blade response is performed in the frequency domain. Therefore, the velocity deficit in the pylon wake is rewritten as a periodic gust in a direction normal to the blade sections' upper surfaces and then expressed as a complex Fourier series.

The harmonics of the unsteady blade lift coefficient due to the change in angle of attack in the pylon wake region $\Delta c_{l_{instk}}^{\Delta \alpha}$ are computed using the Sears function [5, 9]:

$$\Delta c_{l_{instk}}^{\Delta \alpha}(\eta) = 2\pi \frac{v_{gnk}(\eta)}{W_{iso}(\eta)} S \quad (6)$$

with v_{gnk} the Fourier coefficients of the normal gust velocity and S the Sears function as defined in Refs. [22, 21]. A (low-frequency) compressibility correction is applied to the result obtained from the incompressible Sears function [1].

Having computed the harmonics of the unsteady lift coefficient, the local unsteady lift coefficients are obtained as a function of the blade's polar angle ϕ by taking the inverse Fourier transform of the harmonics.

The changes in the lift and drag coefficients due to the effects of the reduced dynamic pressure and the increased angle of attack in the pylon wake region are superimposed to obtain the final unsteady propeller blade loads c_l^{US} and c_d^{US} . With the unsteady blade loads known, the resulting unsteady thrust and torque are obtained by integrating the contributions of all blade elements:

$$T_{1B}^{US}(\phi) = \sum_{i=1}^{N_r} \frac{1}{2} \rho W_i^2 (c_{l_i}^{US}(\phi) \cos \varphi_i - c_{d_i}^{US}(\phi) \sin \varphi_i) c_i \Delta \eta_i R \quad (7)$$

$$Q_{1B}^{US}(\phi) = \sum_{i=1}^{N_r} \frac{1}{2} \rho W_i^2 (c_{l_i}^{US}(\phi) \sin \varphi_i + c_{d_i}^{US}(\phi) \cos \varphi_i) c_i \eta_i \Delta \eta_i R^2 \quad (8)$$

with φ_i the advance angle (including induced effects) of blade segment i . Note that the assumption is made that the additional lift and drag resulting from the installation effects act perpendicular and parallel to the local effective velocity including induced effects.

Having computed the unsteady thrust and torque for a single-bladed propeller using Eqs. 7 and 8, the results are generalized to a B -bladed propeller by taking into account the proper phase shifts between the various blades. Finally, the unsteady thrust and torque are added to the steady-state (isolated) results to obtain the propeller performance in the installed configuration.

4.3 Propeller Noise Emissions

The propeller noise emissions are computed using the methods developed by Hanson [14, 15]. The isolated propeller is analyzed with the scheme discussed in detail in Ref. [14]. For the installed configuration the method for contra-rotating propellers discussed in Ref. [15] is adopted. The current case with a fixed inlet distortion due to the presence of the pylon follows from the contra-rotating problem by assuming an imaginary front rotor with zero angular velocity and unity blade number. In all cases the assumption of a uniform lift distribution was made, while the blade loads obtained from the isolated propeller performance analysis were corrected for the shift due to the induced angle. Broadband noise emissions were neglected in all analyses.

5 Results

The experimental and numerical methods were used to analyze the UBR's outflow velocity pro-

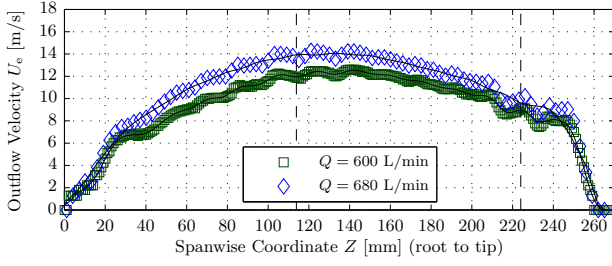


Fig. 9 Uniform Blowing Rod outflow profiles for two blowing rates; $X_w = 0.1c_{pyl}$.

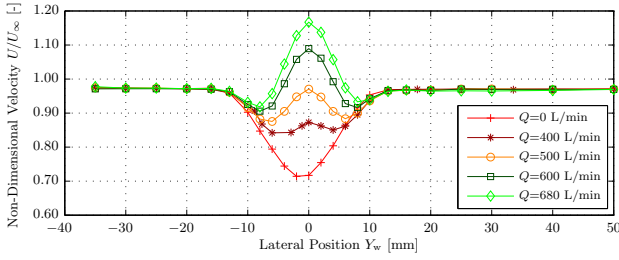


Fig. 10 Pylon wake velocity profiles for various blowing rates; $U_\infty = 19 \text{ m/s}$, $X_w = 0.3c_{pyl}$.

files, the pylon wake profiles, the propeller performance, and the propeller noise emissions.

From Fig. 9 it is observed that the UBR's outflow is not as uniform in spanwise direction as desired. This is likely the result of non-uniform inflow due to flow separation in the divergent inlet of the UBR.

5.1 Pylon Wake Profiles

The velocity profiles measured in the pylon wake at a freestream velocity of $U_\infty = 19 \text{ m/s}$ are presented in Fig. 10. The wake profiles were measured at the position of the propeller plane used in the evaluations of the installed and blown propeller performance and noise emissions (corresponding to a longitudinal wake-based coordinate of $X_w = 0.3c_{pyl}$). The pylon blowing system was operated for a number of blowing rates Q ranging from zero (unblown) up to the maximum blowing rate of 680 L/min. Note that the wake profiles were obtained for the isolated pylon, i.e. the presence of the propeller was neglected.

The non-dimensional wake velocity profiles displayed in Fig. 10 show a continuously increasing reduction in wake depth with increasing blowing rate. At blowing rates of 500 and

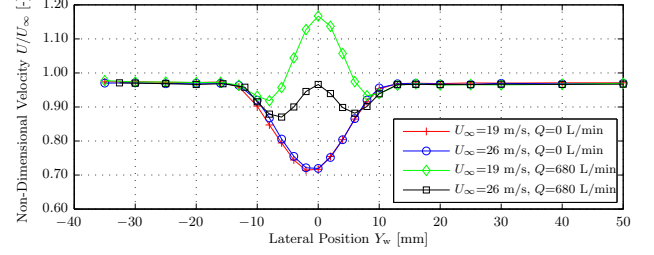


Fig. 11 Unblown and blown pylon wake velocity profiles for different freestream velocities; $X_w = 0.3c_{pyl}$.

600 L/min a reduction in the integrated velocity deficit of around 60% is obtained when compared to the unblown configuration. The application of blowing from the extended pylon's trailing edge does not have an appreciable effect on the total wake width. This indicates that the jet blown into the flow from the UBR's outlet does not fully mix with the external flow before reaching the axial position of $X_w = 0.3c_{pyl}$. As a result, the velocity profiles measured at this position are not uniform but instead display a profile with one local maximum on the wake's centerline and two local minima left and right of the centerline.

The influence of the freestream velocity on the amount of wake fill-up achieved using the pylon blowing system is shown in Fig. 11, which contains data measured at 19 m/s and 26 m/s.

Figure 11 shows that the amount of wake fill-up obtained by applying the blowing system decreases with increasing freestream velocity. At a given blowing rate the increase in the non-dimensional velocity on the wake centerline is smaller when the freestream velocity is higher. This is directly related to the ratio of the freestream flow velocity and the velocity of the flow blown into the pylon wake. The latter needs to be larger than the freestream velocity for the blowing system to be effective.

5.2 Propeller Performance

The propeller performance was analyzed to assess the effects of installation and pylon blowing on pusher propeller performance. The performance was expressed in terms of the thrust coefficient C_T , the torque coefficient C_Q , and the pro-

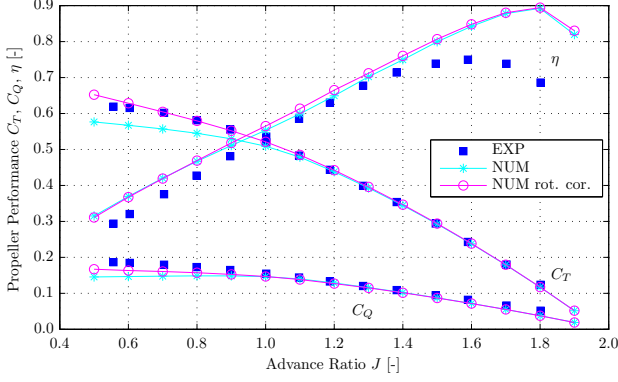


Fig. 12 Experimental and numerical propeller performance diagrams; isolated configuration, $U_\infty = 26 \text{ m/s}$, showing the effect of rotation correction according to eq. (3).

propeller efficiency η , defined as:

$$C_T = \frac{T}{\rho n^2 D^4} \quad (9)$$

$$C_Q = \frac{Q}{\rho n^2 D^5} \quad (10)$$

$$\eta = \frac{J C_T}{2\pi C_Q} \quad (11)$$

with D the propeller diameter, J the advance ratio ($J = \frac{U_\infty}{nD}$), n the rotational rate of the propeller in revolutions per second, Q the torque, and T the thrust.

The RSB used to acquire the experimental data suffered from a low signal-to-noise ratio due to interference effects with electromagnetic radiation from the wind tunnel motor. As a result, time-accurate experimental evaluations were not possible. The time-averaged measurement data on the other hand proved to be reproducible. To remove high frequency noise from the experimental data a zero-phase digital filter with cut-off frequency of 2500 Hz was used.

5.2.1 Isolated Configuration

The computed and measured propeller performance diagrams for the isolated configuration are depicted in Fig. 12.

As expected a quasi-linear behavior is found for high advance ratios, while at the lower advance ratios the non-linear blade section response

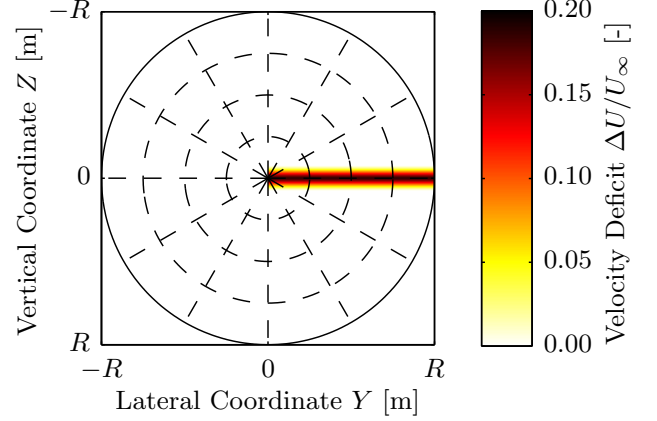


Fig. 13 Velocity deficit at the position of the propeller plane; $U_\infty = 26 \text{ m/s}$, $X_w = 0.3c_{\text{pyl}}$.

results in a non-linear behavior. Excellent agreement is obtained between the experimental and numerical results for the thrust coefficient, with differences of at most 1% for advance ratios above $J = 0.7$. The larger differences at lower advance ratios are as expected considering the high blade angles of attack experienced in this regime, reducing the accuracy of the numerical analysis of the blade section characteristics. The correspondence between the computed and measured torque coefficients is not as good as for the thrust coefficient. This is likely the result of inaccuracies in the drag coefficient data used in the XROTOR computations.

5.2.2 Installed Configuration

Based on the physics of the pylon - pusher propeller interaction it can be expected that the time-averaged thrust and torque increase in the installed configuration. When rotating through the pylon wake the propeller blades experience an increase in angle of attack resulting from the locally reduced inflow velocity. This leads to an increase in lift produced by the blade in the wake region, resulting in distinct peaks in the thrust and torque signals. Note that this increase is partially offset by the reduction in dynamic pressure in the pylon wake. To illustrate the extent of the pylon wake region on the propeller disk, Fig. 13 presents an example of a computed velocity deficit profile at the position of the propeller plane.

The propeller inflow depicted in Fig. 13 was used to compute the installed propeller performance according to the methods outlined in Section 4.2. The experimental data are not treated here since the measured data sets showed an inconsistent behavior between results obtained at different freestream velocities. This is likely the result of the fact that the small changes in the propeller performance due to installation fell within the expected variability of the measurements performed using the RSB.

A comparison between the numerical isolated and installed propeller performance is presented in Fig. 14.

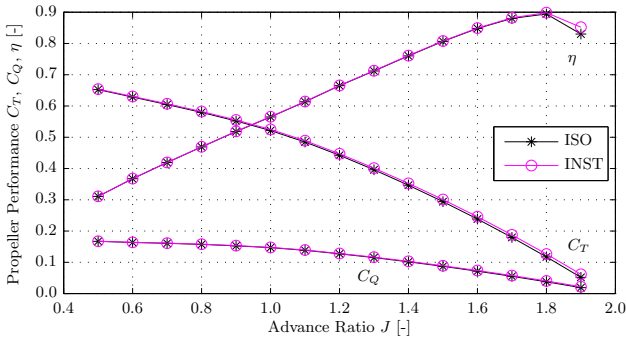


Fig. 14 Computed effects of pylon installation on the propeller performance. Isolated (ISO) and installed (INST) configurations, $U_\infty = 26\text{ m/s}$.

From Fig. 14 it is clear that the effects of installation on the time-averaged propeller performance are small. For advance ratios below $J = 1.4$ the increase in the thrust coefficient due to installation is less than 2% of the isolated value. For the same advance ratio range the time-accurate thrust and torque signals displayed peak-to-peak variations of less than 4%. The small effects of installation on the propeller performance are as expected considering the limited extent of the polar region in which the pylon wake is present.

5.2.3 Blown Configuration

The propeller performance in the blown configuration was computed with the same methods as used for the installed configuration, but now with a measured blown pylon wake profile (corresponding to the profile at $Q = 600\text{ L/min}$ shown

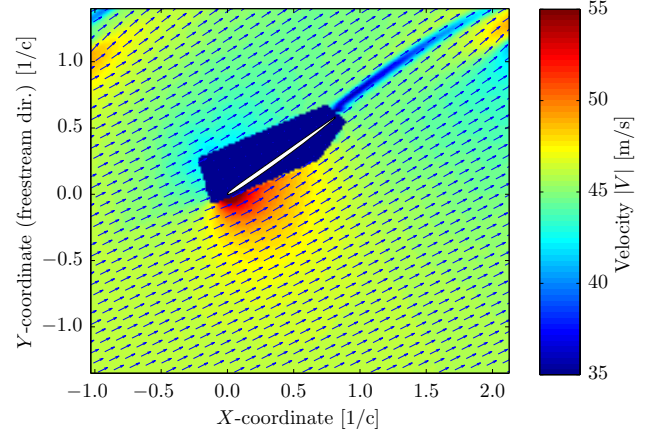


Fig. 15 Velocity field obtained from PIV measurements in a fixed frame of reference at $r/R = 0.87$ and $J = 1.3$.

in Fig. 10) as input. It was found that the application of pylon blowing further reduces the effects of the presence of the pylon on the propeller performance. For the same advance ratio range as considered before ($J < 1.4$), the computed time-averaged thrust and torque coefficients in the blown configuration were equal to their isolated counterparts. The corresponding peak-to-peak variations in the time-accurate blown propeller performance results displayed fluctuations of at most 2%.

5.3 PIV analysis

PIV was performed to obtain velocity fields around the propeller blade which could be used for additional analyses. In this case the velocity data were used to determine the lift coefficient at different radial positions by computing the local circulation via a contour integration around the propeller blade.

Fig. 15 shows a typical example of the velocity field as determined by the PIV measurements. The dark blue area around the airfoil corresponds to a masked area that was removed to prevent unwanted effects from erroneous datapoints (due to reflections) close to the blade surface. To obtain velocity data in the shadow region, in front of the airfoil, interpolation was performed. From Fig. 15 both the periodicity in azimuthal direction and the wake area can clearly be recognized.

The radial distribution of the blade lift coef-

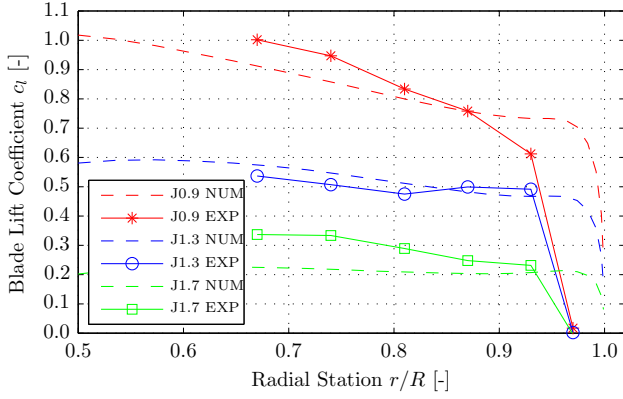


Fig. 16 Radial distribution of the blade lift coefficient. Comparison of experimental values obtained from PIV data and computed results.

efficient computed from the PIV data is presented in Fig. 16. The zero values close to the tip of the propeller are very likely indicative for the contraction of the slipstream that is not accounted for in the numerical propeller model. The cause for the relatively large discrepancy between numerical and experimental data for an advance ratio of $J = 1.7$ is yet unclear to the authors.

5.4 Propeller Noise Emissions

As mentioned previously, the unsteady blade loads resulting from the installation of the pylon upstream of the propeller lead to additional noise emissions. Application of the pylon blowing system should fill up the pylon wake, thereby reducing the noise penalty due to installation. To assess the magnitude of the noise penalty due to installation and to verify whether the pylon blowing system could indeed result in reduced noise levels, the propeller noise emissions were computed and measured in the isolated, installed, and blown configurations. The experimental total noise levels were obtained by extracting the SPL of the first ten propeller tones and subsequently summing these.

5.4.1 Unblown Configuration

The propeller noise emissions in the installed configuration are shown as a function of the advance ratio in Fig. 17. Both the experimental and numerical data are considered.

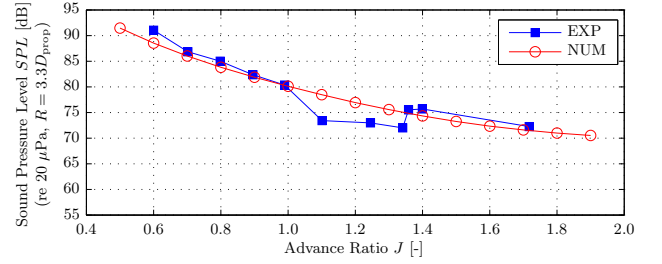


Fig. 17 Total sound pressure levels versus advance ratio; installed configuration, $U_\infty = 19 \text{ m/s}$, $\theta = 110^\circ$, $\phi = 90^\circ$.

As can be seen, a good agreement is obtained between the numerical and experimental data over the entire advance ratio range. However, the experimental data show a distinct drop in noise levels for the advance ratio range $1.0 \leq J \leq 1.3$. This is likely the result of cancellation of the sound fields associated with the steady and unsteady blade loads.

A comparison between the isolated and installed noise levels at an axial directivity angle of $\theta = 110^\circ$ (see Fig. 20, presented in the discussion of the blown results) shows that the installation of the pylon upstream of the propeller significantly increases the propeller noise emissions. Depending on the advance ratio, noise increases of up to 15 dB were measured. Note that in the advance ratio range $1.0 \leq J \leq 1.3$, the isolated noise levels are higher than the installed values. This corresponds to the observation, made before, that in this advance ratio range the installed noise levels show a distinct drop due to cancellation of the sound fields associated with the steady and unsteady blade loads.

The effects of installation significantly change the directivity pattern of the propeller noise emissions. Computations performed at a freestream velocity of 50 m/s led to the axial and circumferential directivity patterns of the sound pressure levels of the propeller noise as depicted in Fig. 18 and Fig. 19, respectively. Again the SPL was defined at an observer distance of 3.3 times the propeller diameter.

Figure 18 displays that the effects of installation of the upstream pylon are especially pronounced in the up- and downstream directions. Whereas for the isolated propeller the noise emis-

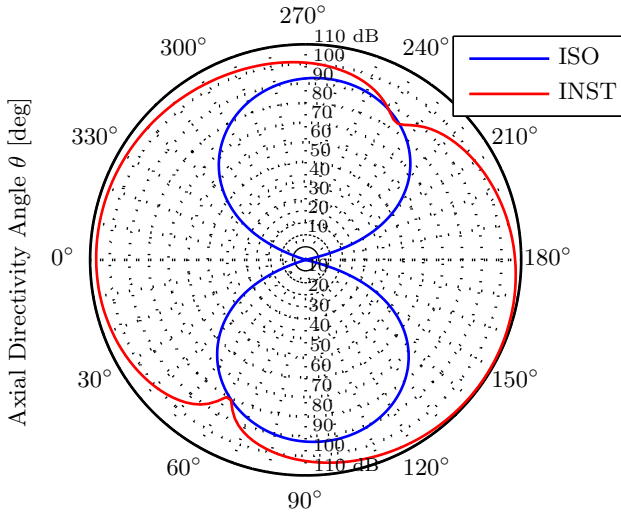


Fig. 18 Computed axial directivity of isolated and installed noise emissions; $U_\infty = 50\text{ m/s}$, $J = 0.9$, $\phi = 90^\circ$.

sions vanish towards the propeller axis, in the installed configuration this is no longer the case. Furthermore, the installation of the pylon introduces distinct lobes in the circumferential direction as shown in Fig. 19. The installed noise levels are highest in the circumferential range approximately perpendicular to the pylon plane.

5.4.2 Blown Configuration

The goal of the pylon blowing system is to fill up the pylon wake, thereby reducing the installation effects hence reducing the propeller noise emissions compared to the unblown case. To verify whether application of the pylon blowing system indeed led to noise reductions Fig. 20 presents the measured noise levels in the isolated, installed, and blown ($Q = 660\text{ L/min}$) configurations.

Figure 20 shows that the application of the pylon blowing system indeed reduced the propeller noise emissions. Depending on the advance ratio noise reductions due to blowing of up to 7 dB are observed when compared to the unblown, installed configuration. In general the propeller noise emissions in blown conditions are still higher than for the isolated configuration, indicating that the installation effects are not completely eliminated by the application of blowing. This is as expected considering the blown pylon

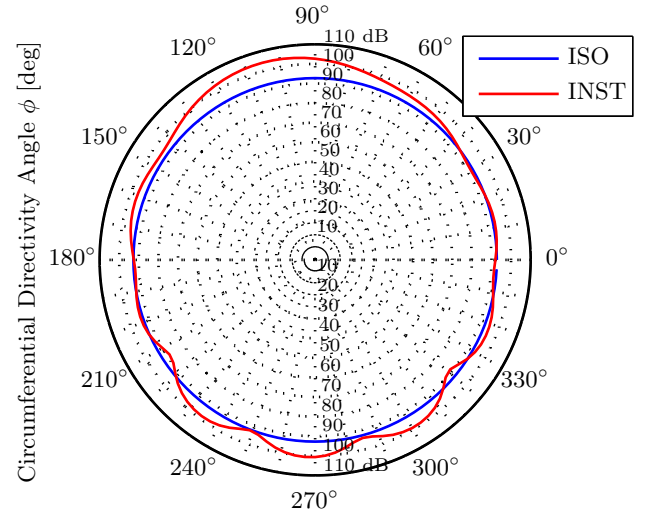


Fig. 19 Computed circumferential directivity of isolated and installed noise emissions; $U_\infty = 50\text{ m/s}$, $J = 0.9$, $\theta = 90^\circ$.

wake profiles discussed before, which did not become completely uniform due to insufficient mixing of the external and blown flows.

All noise results discussed so far considered the combination of all propeller tones. Furthermore, only a single blowing rate was considered. To further increase insight in the effects of blowing on the propeller noise emissions, Fig. 21 presents the tonal noise reductions measured at all blowing rates considered, for the first six propeller tones separately. Note that these values are only valid for a single operating point ($U_\infty = 19\text{ m/s}$ and $J = 0.9$). The orange dashed lines indicate the expected variability in the noise measurements.

From Fig. 21 it is concluded that the applica-

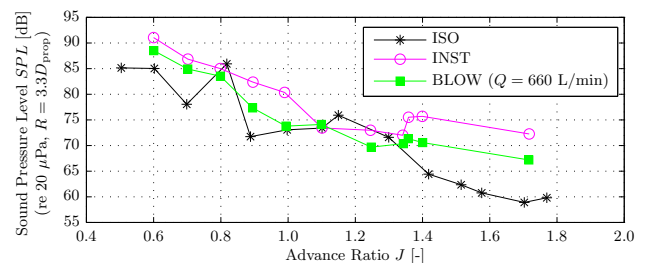


Fig. 20 Total sound pressure levels versus advance ratio (experimental results); isolated, installed, and blown configurations, $U_\infty = 19\text{ m/s}$, $\theta = 110^\circ$, $\phi = 90^\circ$.

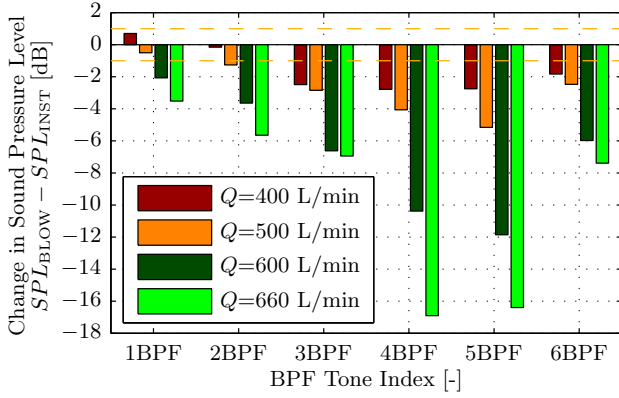


Fig. 21 Tonal noise reductions due to blowing: effects of the blowing rate; blown configuration, $U_\infty = 19\text{ m/s}$, $J = 0.9$, $\theta = 110^\circ$, $\phi = 90^\circ$.

tion of blowing reduces the sound pressure levels of the tones for all but one of the blowing rates considered. The SPL of the propeller tones decreases with increasing blowing rate, with the reductions becoming significant for all six tones at the blowing rates of 600 and 660 L/min. When blowing at a rate of 660 L/min the 1BPF tone is reduced by almost 4 dB, while the reductions for the higher BPF multiples are even larger.

Considering the wake profiles presented in Fig. 10 it might be surprising that the largest noise reductions were achieved at $Q = 660\text{ L/min}$. The wake measurements showed that at a comparable blowing rate ($Q = 680\text{ L/min}$) the application of blowing resulted in the introduction of a jet with higher than freestream velocity in the center of the wake region. However, it should be noted again that the wake measurements were performed using the isolated pylon model only. With the thrusting propeller present, the external velocity at the position of the blowing outlet will be increased. Considering that the effectiveness of the blowing system reduces with increasing external flow velocity (see Fig. 11), it is concluded that it might be the case that the locally increased velocities ahead of the thrusting propeller demand a higher blowing rate to fill up the pylon wake than required for the isolated case. As such, it might be possible that in powered conditions the wake profile at the propeller plane shows a minimum integral velocity deficit for a blowing rate of $Q = 660\text{ L/min}$, thereby

explaining the best performance at this blowing rate. To test this hypothesis wake surveys should be performed with the rotating propeller present behind the pylon.

It is expected that there exists a certain blowing rate for which the noise reductions due to blowing display a maximum, after which the noise levels increase again for higher blowing rates. Considering that the noise levels continued to decrease with increasing blowing rate for all blowing rates considered, it is concluded that the most effective blowing rate might not have been reached. Additional tests should be performed at higher blowing rates to verify this.

6 Conclusions

Experimental and numerical analyses of the effects of pylon blowing on pusher propeller performance and noise emissions have been performed successfully. From the results obtained so far the following conclusions can be drawn:

- Application of the pylon blowing system resulted in reductions in the integrated velocity deficit of up to 60% compared to the unblown configuration. However, the mixing of the external and blown flows was not optimal, as a result of which the velocity profiles in blown conditions were not completely uniform.
- The agreement between the experimental and numerical propeller performance for the isolated configuration was good, with differences between the computed and measured thrust coefficients smaller than 1% for advance ratios above 0.7. It was concluded that the effects of installation on the time-averaged propeller performance are small, with increases in the thrust and torque coefficients due to installation of less than 2% for advance ratios below 1.4. Accordingly, it was found that the effects of blowing on the time-averaged propeller performance are small.
- PIV measurements around the propeller blade basically confirmed the loading dis-

tributions that were found from the numerical model. However, no explanation for discrepancies at the large advance ratio of $J = 1.7$ was found, so far.

- From the experimental and numerical evaluations of the propeller noise emissions it is concluded that the installation of an upstream pylon strongly increases the noise levels, with measured noise penalties of up to 15 dB compared to the isolated case. The pylon blowing system was successful in reducing the propeller noise emissions compared to the unblown case. Depending on the advance ratio noise reductions of up to 7 dB were observed. Considering that the noise reductions increased with increasing blowing rate, it was concluded that the most effective blowing rate might not have been reached during the experiments.

The results presented in this paper confirm the potential of pylon trailing edge blowing to reduce the adverse installation effects experienced by pusher propellers. Considering the significant fuel savings promised by future engine concepts employing propellers in a pusher configuration, this is an important result which can be used to develop potential solutions for the relatively high noise emissions associated with such propulsion systems. Follow-up research using additional computational and measurement techniques is required to increase the understanding of the mixing characteristics of the blowing system and its effects on the propeller performance and noise emissions.

Acknowledgments

The authors would like to thank Christian Potma from FlowMotion for the efforts he put into the design of the “Uniform Blowing Rod”, a device which was essential for the successful completion of the experimental test campaigns. Furthermore, DNW is kindly acknowledged for providing the propeller test rig under a lease contract with Delft University of Technology.

References

- [1] R. K. Amiet. Compressibility Effects in Unsteady Thin-Airfoil Theory. *AIAA Journal*, 12(2):252–255, 1974.
- [2] P. J. W. Block. Experimental Study of the Effects of Installation on Single- and Counter-Rotation Propeller Noise. 1986. NASA-TP-2541.
- [3] P. J. W. Block. Pusher Propeller Noise Directivity and Trends. *10th AIAA Aeroacoustics Conference*, 1986. Seattle, WA, USA.
- [4] P. J. W. Block and G. L. Gentry, Jr. Directivity and Trends of Noise Generated by a Propeller in a Wake. 1986. NASA-TP-2609.
- [5] Y. Colin, A. Carazo, B. Caruelle, T. Nodé-Langlois, and A. B. Parry. Computational strategy for predicting CROR noise at low-speed - Part I: review of the numerical methods. *18th AIAA/CEAS Aeroacoustics Conference (33rd AIAA Aeroacoustics Conference)*, 2012. Colorado Springs, CO, USA.
- [6] Delft University of Technology. Open Jet Facility, 2008. [Online] Available at: www.lr.tudelft.nl/en/organisation/departments-and-chairs/aerodynamics-and-wind-energy/wind-energy/facilities/open-jet-facility/ [Accessed 15 November 2012].
- [7] M. Drela and H. Youngren. XFOIL: An Analysis and Design System for Low Reynolds Number Airfoils, 2008. [Software] Available at: <http://web.mit.edu/drela/Public/web/xfoil/> [Accessed 15 November 2012].
- [8] M. Drela and H. Youngren. XROTOR: an interactive program for the design and analysis of ducted and free-tip propellers and windmills, 2011. [Software] Available at: <http://web.mit.edu/drela/Public/web/xrotor/> [Accessed 15 November 2012].
- [9] M. H. Dunn and A. F. Tinetti. Advanced Time Domain Noise Prediction Methods for Open Rotors and Installation Effects. *18th AIAA/CEAS Aeroacoustics Conference (33rd AIAA Aeroacoustic Conference)*, 2012. Colorado Springs, CO, USA.
- [10] D. M. Elliott. Initial Investigations of the Acoustics of a Counter-Rotating Open Rotor Model With Historical Baseline Blades in a Low-Speed Wind Tunnel. 2012. NASA-TM-

- 2012-217258.
- [11] E. Envia. NASA Open Rotor Research. *14th CEAS-ASC Workshop*, 2010. Warsaw, Poland.
- [12] S. Funke, L. Kim, and H. A. Siller. Microphone-Array Measurements of a Model Scale Contra-Rotating Open Rotor in a Reverberant Open Wind-Tunnel. *17th AIAA/CEAS Aeroacoustics Conference (32nd AIAA Aeroacoustics Conference)*, 2011. Portland, OR, USA.
- [13] G. L. Gentry, Jr., E. R. Booth, Jr., and M. A. Takkallu. Effect of Pylon Wake With and Without Pylon Blowing on Propeller Thrust. 1990. NASA-TM-4162.
- [14] D. B. Hanson. Helicoidal Surface Theory for Harmonic Noise of Propellers in the Far Field. *AIAA Journal*, 18(10):1213–1220, 1980.
- [15] D. B. Hanson. Noise of Counter-rotation Propellers. *Journal of Aircraft*, 22(7):609–617, 1985.
- [16] T. J. Mueller, editor. *Aeroacoustic Measurements*. Berlin, Germany: Springer-Verlag Berlin Heidelberg New York, 2002.
- [17] P. M. Niskode, R. Stickles, B. Allmon, and R. DeJong. CLEEN Consortium Open Session, October 2010. [Online] Available at: www.faa.gov [Accessed 29 September 2012].
- [18] N. Peake and A. B. Parry. Modern Challenges Facing Turbomachinery Aeroacoustics. *Annual Review of Fluid Mechanics*, 44:227–248, 2012.
- [19] J. Ricouard, E. Julliard, M. Omaïs, V. Regnier, S. Baralon, and A. B. Parry. Installation effects on contra-rotating open rotor noise. *16th AIAA/CEAS Aeroacoustics Conference*, 2010. Stockholm, Sweden.
- [20] H. Schlichting and K. Gersten. *Boundary-Layer Theory*. Springer, Heidelberg, 8th (revised and enlarged) edition, 2000.
- [21] W. R. Sears. *A Systematic Presentation of the Theory of Thin Airfoils in Non-Uniform Motion*. PhD thesis, California Institute of Technology, 1938.
- [22] W. R. Sears. Some Aspects of Non-Stationary Airfoil Theory and Its Practical Application. *Journal of the Aeronautical Sciences*, 8(3):104–108, 1941.
- [23] B. Shivashankara, D. Johnson, and R. Cuthbertson. Installation effects on counter rotating propeller noise. *13th AIAA Aeroacoustics Conference*, 1990. Tallahassee, FL, USA.
- [24] H. Snel, R. Houwink, and J. Bosschers. Sectional Prediction of Lift Coefficients on Rotating Wind Turbine Blades in Stall. *Netherlands Energy Research Foundation (ECN) Internal Report*, 1994. ECN-C-93-052.
- [25] A. Stürmer and J. Yin. Aerodynamic and Aeroacoustic Installation Effects for Pusher-Configuration CROR Propulsion Systems. *28th AIAA Applied Aerodynamics Conference*, 2010. Chicago, IL, USA.
- [26] A. Stürmer and J. Yin. DLR-AS CROR & Propeller Noise Prediction. *14th CEAS-ASC Workshop*, 2010. Warsaw, Poland.
- [27] R. P. J. O. M. van Rooij. Modification of the boundary layer calculation in RFOIL for improved airfoil stall prediction. 1996. Report IW-96087R.
- [28] R. P. Woodward and C. E. Hughes. Noise of a Model Counterrotation Propeller With Simulated Fuselage and Support Pylon at Take-off/Approach Conditions. *12th AIAA Aeroacoustics Conference*, 1989. San Antonio, TX, USA.

Copyright Statement

The authors confirm that they, and/or their company or organization, hold copyright on all of the original material included in this paper. The authors also confirm that they have obtained permission, from the copyright holder of any third party material included in this paper, to publish it as part of their paper. The authors confirm that they give permission, or have obtained permission from the copyright holder of this paper, for the publication and distribution of this paper as part of the ICAS2014 proceedings or as individual off-prints from the proceedings.